Gravity waves retrieval from sea surface elevation images using convolution neural network

Submitted by: Eilam Golan, Giora Hasson, and Krishanu Kumar.

Supervised by: Dr. Yaron Toledo and Mr. Nir Haim.

1. Introduction

1.1 Description of Problem

In the present analysis, a numerical model is used to create sea surface elevation images based on the wave propagation direction θ_0, wave spectra and directional spreading function. The wave propagation direction θ_0 is varied from -30° to -30° and the wave spectra are defined by the spectrum peak's wavenumber, which varied from 0.02 to 0.1 rad/m in this project's simulations. The set of sea surface elevation images are divided into three segments, i.e., training, validation, and test data. The training data is used for the initial training of the convolutional neural network (CNN), based on which a model is generated. The validation set is given as an input to the model to analyze the accuracy of the model to predict the wavenumber k based on these images.

Based on the training sets, three different models are generated. The first model is only given the images of sea surface elevation with θ_0 = 0°, the second model is given images with θ_0 = 0° and 30°, and the third model is given the images of sea surface elevation images with $\theta_0 = 0 \pm 5°$ as an input. The three different models are used to predict the sea surface elevation of different wavenumbers and random angle of propagation between $-30° < \theta_0 < 30°$ and the accuracy of these models are compared.

1.2 Project Objective

- To create 10,000 images of sea surface elevation of θ_0 = 0° and 30° each for random gravity wave spectra.
- To create 10,000 images of sea surface elevation of $\theta_0 = 0 \pm 5°$ each for random gravity wave spectra.
- Divide these images into three different data sets i.e., training, validation, and test data.
- Create 10,000 images of sea surface elevation for $-30° < \theta_0 < 30°$ and random gravity wave spectra.
- Train different models based on these images, and angle of propagation and compare the accuracy to predict wavenumber k and angle of propagation θ_0 based on randomly generated images for $-30° < \theta_0 < 30°$.

1.3 Literature survey

The ability to predict sea conditions has myriad advantages, which could be utilized for offshore operations, oceanography, climate science, sustainable energy production, and aqua culturing [1,2]. Also, the sea-based infrastructure such as oil rigs, sea-ports, power plants, etc., depends heavily on the wave condition to maintain their day-to-day operations.

The waves typically observed in the ocean are called gravity waves or wind waves. These waves are generated due to the disturbance created on the interface of the water surface. The surface is displaced from the position of equilibrium, and gravitational force tries to maintain the position of equilibrium, causing a movement of forth and back which is known as wave orbit [3]. The wind produces small waves of few centimeters in length, and the wind over the surface produces pressure difference along the wave causing wave growth, which leads to an exponential growth of wave amplitude, and wave interaction lead to the formation of longer waves [4]. The gravity waves can be characterized based on period range $0.3 < T < 30$ sec [5], angular frequency $0.2 < \omega < 20$ rad/s, wavenumber $4.5e\text{-}3 < k < 45$ rad/m, and wavelength $0.14 < \lambda < 1400$ m. The spectral energy density of sea waves is represented as a function of frequency or wavenumber defined as the JONSWAP power spectrum.

Currently, the sea surface elevation is measured using numerous techniques such as wave gauges, wave buoy, video camera, radars, and satellite images. These data are used as an input for forecasting wave conditions for models based on statistical techniques or physics-based models [6,7]. However, traditionally used physics-based models are imperfect, computationally expensive, and the resolution of these models is not high enough to resolve the small-scale data, and hence there is a disagreement between the forecasted data and observation data of the ocean. These issues are addressed by the introduction of machine learning for wave conditions predictions which has high-resolution as well as computationally inexpensive. Machine learning has been used in weather prediction [8], climate study [9], and atmospheric process study [10]. The deep neural network is also used to develop Reynolds-averaged turbulence model [11,12], which also respects the physical properties of the system, i.e., conservation of mass, momentum, etc. as well as it is data-driven, which reduces the computational cost and is significantly accurate. However, using a deep neural network or convolutional neural network (CNN) to predict ocean conditions is not new. The prime focus of this study is to analyze the accuracy of different models that are developed using different sets of training data and input. The aim is to analyze the importance of input information on the accuracy of the predictions made by the model. The details about the numerical model and convolution neural network used in the analysis are discussed in detail in chapter 2.

2. Methods

2.1 Linear Water Wave Theory

Two important parameters to describe waves are their length and height. The water depth is also an important parameter that helps determine other important parameters of the wave. From these three parameters, all the other wave parameters can be determined theoretically [13]. A two-dimensional schematic description of a wave propagating in the x-direction is presented in Figure 1 [13].

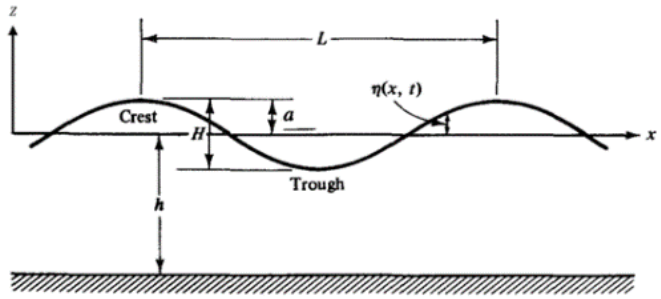

Figure 1. Schematic representation of the main wave elements and their numerical characteristics, such as wavelength, height, and amplitude [13].

The length of the wave, L, is the horizontal distance between two successive wave crests, or the distance between two wave troughs, along the propagation direction of the wave. The still water line defines as $z = 0$, and the wave equation, η, refers to the vertical distance from the still water line to the water surface, as a variable of space and time. The depth, h, is the vertical distance from the bottom of the sea to the still water line. The wave amplitude, a, is the vertical distance from $z = 0$ to the wave crest (can also be defined appropriately according to the wave trough), and the wave height, H, is the distance between the wave trough and crest. The wave period T, is the time required for two successive crests or troughs to pass a particular point.

Two other wave parameters can be defined from the parameters given in the previous paragraph. The ordinary frequency of the wave, f, and the angular frequency, ω. The ordinary frequency is the number of cycles per unit, and the relation between it and the period is given by:

$$f = \frac{1}{T}\ [Hz] \qquad \text{Eq. 1}$$

and the angular frequency, ω, describes the phase change rate. The relation between the angular frequency and the ordinary frequency is given by:

$$\omega = 2\pi f\ [rad] \qquad \text{Eq. 2}$$

hence the relation with the wave period is:

$$\omega = \frac{2\pi}{T}\left[\frac{rad}{m}\right] \qquad \text{Eq. 3}$$

The wavenumber, k, is the spatial frequency of the wave. Whereas temporal frequency can be thought of as the number of waves per time unit, wavenumber (spatial frequency) is the number of waves per distance unit. The wavenumber relation to the wavelength can be written as:

$$k = \frac{2\pi}{L}\left[\frac{rad}{m}\right] \qquad \text{Eq. 4}$$

Dispersion relations generally describe the effect of dispersion in a medium on a wave's properties, traveling within that medium. A dispersion relation relates the wavenumber (or wavelength) of a wave to its frequency and describes the phenomenon that waves with different wavenumbers travel at different phase speeds. The dispersion relation of water waves is given as:

$$\omega^2 = gk\tanh(kh)\left[\frac{rad^2}{s^2}\right] \qquad \text{Eq. 5}$$

The region is defined as shallow water when $kh < \pi/10$ rad. In this case $\tanh(kh) \approx kh$, and accordingly, the dispersion relation can be approximated to:

$$\omega^2 = gk^2h\left[\frac{rad^2}{s^2}\right] \qquad \text{Eq. 6}$$

The region is defined as deep water when $\pi < kh$ rad. In this case $\tanh(kh) \approx 1$, and accordingly, the dispersion relation can be approximate to:

$$\omega^2 = gk\left[\frac{rad^2}{s^2}\right] \qquad \text{Eq. 7}$$

For a single wave that is propagating in space in a single consistency direction, the surface elevation can be described by the following formula:

$$\eta(x, y, t) = a\cos\left(k_x x + k_y y - \omega t + \varphi\right)\ [m] \qquad \text{Eq. 8}$$

when x and y are the spatial coordinates, t is the time, ω is the frequency, φ is the wave phase, a is the wave amplitude, and k_x and k_y are the two components of the wavenumber vector. Waves in nature rarely appear to look the same from wave to wave, nor do they always propagate in the same direction. If a device to measure the water surface elevation (sea surface elevation), η; as a function of time, was placed on a platform in the middle of the ocean, it might obtain a record such as that shown in Figure 2.

Figure 2. Example of a possible recorded waveform [13].

This sea can be seen as a superposition of many sinusoids going in different directions. For a simple example, consider two different sine waves that propagate in the same direction, the actual wave will be the sum of them, as a superposition of two sinusoidal waves. The next figure illustrates the example.

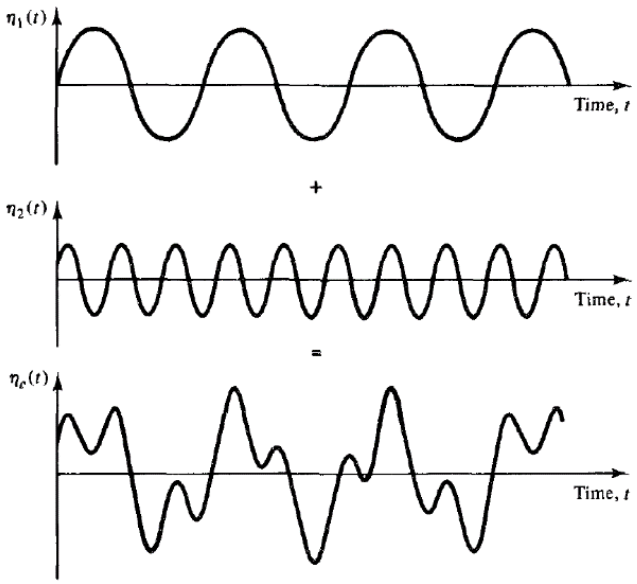

Figure 3. Example of a complex waveform obtained as a sum of two sinusoids [13].

The sea surface elevation can be described as a superposition of many waves and can be defined as the sea surface elevation by the following sum of harmonic functions:

$$\sum_{i=1}^{N_k} \eta(x,y,t) = a_i \cos\left((k_x)_i x + (k_y)_i y - \omega_i t + \varphi_i\right) \ [m] \qquad \text{Eq. 9}$$

when every single wave is characterized with a wavenumber, frequency, and phase, so that N_k is the number of harmonic waves that composed the sea surface.

As mentioned above, the actual sea surface is composed of a large variety of waves moving in different directions and with different frequencies, phases, and amplitudes. Moreover, unfortunately, there is a great amount of randomness in the sea, so statistical techniques need to be brought to bear. This characterization of sea surface requires a method that can reference wave heights. To explain the meaning of such a method, consider a group of N wave heights measured at one point, ordered from largest to the smallest, and assigned numbers from 1 to N. Accordingly, the significant wave height, H_s, is defined as the mean wave height of the highest third of the waves (the highest $N/3$ of the waves).

2.2 Gravity Waves Power Spectrum

In general, the power spectrum of a time series describes the distribution of power into frequency components composing that signal. According to Fourier's analysis, any physical signal can be decomposed into several discrete frequencies or a spectrum of frequencies over a continuous range. The statistical average of a certain signal, as analyzed in terms of its frequency content, is called its spectrum. When the energy of the signal is concentrated around a finite time interval, especially if its total energy is finite, one may compute the energy spectral density. Therefore, the power spectrum then refers to the spectral energy distribution, and accordingly, a summation or integration of the spectral components yields the total power. The waves on the sea surface are not simple sinusoids but a composition of random waves of various lengths and periods. The wave power spectrum can be used to describe this complex surface. The wave spectra give the distribution of wave energy among different wave frequencies, and the spectrum width, peak frequency, peak wavelength, significant height, and other wave parameters can be retrieved from it.

Ocean wind waves are produced by the wind. The faster the wind, the longer the wind blows, and the bigger the area over which the wind blows, the bigger the waves. Pierson-Moskowitz assumed that if the wind blew steadily for a long time over a large area, the waves would come into equilibrium with the wind. They developed the wave power spectrum for a fully developed sea (a sea produced by winds blowing steadily over hundreds of miles for several days) [14]. To obtain a spectrum of a fully developed sea for various wind speeds, they used measurements of waves when the wind had blown steadily for long times over large areas.

Newer research has found that the wave spectrum never becomes fully developed, but rather continues to develop through wave-wave interactions even for very long times and distances. Hence an extra factor was added to the Pierson-Moskowitz spectrum to improve the determination of the gravity wind wave spectrum. As a result of this research, the JONSWAP spectrum was developed [4]. The JONSWAP spectrum is thus a Pierson-Moskowitz spectrum multiplied by an extra peak enhancement factor. The JONSWAP spectrum of sea surface composed of gravity waves, each for a different wind speed is shown in Figure 4.

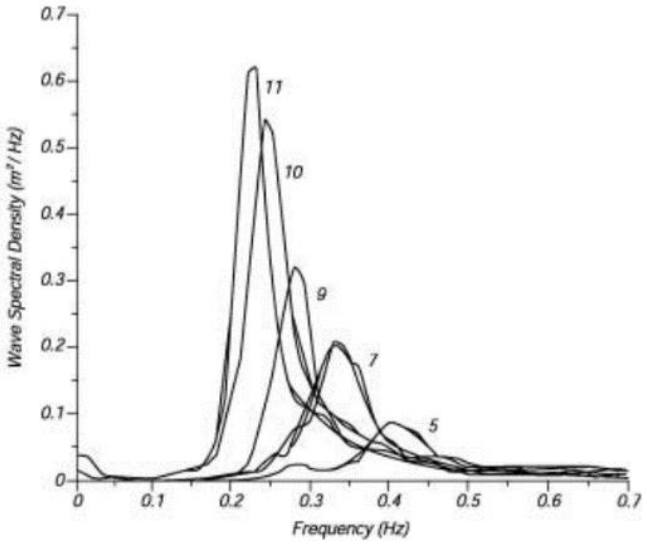

Figure 4. JONSWAP spectrum [4].

The formula of the JONSWAP spectrum is given by:

$$S(\omega) = \frac{\alpha g^2}{\omega^5} \exp\left[-\beta\left(\frac{\omega_p}{\omega}\right)^4\right] \gamma^r \left[\frac{m^2}{Hz}\right] \qquad \text{Eq. 10}$$

when γ^r is the extra factor that was added to the Pierson-Moskowitz model to get the JONSWAP model, α is the

intensity of the spectra that usually taken as $8.1 \cdot 10^{-3}$, β is a shape factor that equals to 1.25, γ is the peak enhancement factor that is usually taken as 3.3, ω_p is the frequency of the peak wave, g is the gravity, r is given by:

$$r = \exp\left[-\frac{\omega - \omega_p}{2\sigma^2\omega_p^2}\right] \quad \text{Eq. 11}$$

and σ is the standard deviation, and it can get two values as given by:

$$\sigma = \begin{cases} 0.07 & \omega \leq \omega_p \\ 0.09 & \omega > \omega_p \end{cases} \quad \text{Eq. 12}$$

JONSWAP spectrum formula can also be defined as the function of the wavelength, k, the dispersion relation, or its approximations for deep water is used and we get:

$$S(k) = A_J \tilde{S}(k) \left[\frac{m^2}{Hz}\right] \quad \text{Eq. 13}$$

where A_J is the normalization parameter and defined by:

$$A_J = \left(\frac{H_s}{4\left(\int_0^\infty \tilde{S}\, dk\right)^2}\right)^2 \quad \text{Eq. 14}$$

$\tilde{S}(k)$ is results to be:

$$\tilde{S}(k) = \frac{1}{2k^3}\exp\left[-\beta\left(\frac{k_p}{k}\right)^2\right]\gamma^r \left[\frac{m^2}{Hz}\right] \quad \text{Eq. 15}$$

where r and the standard deviation σ, is given as:

$$r = \exp\left[-\frac{k^{0.5} - k_p^{0.5}}{2\sigma^2 k_p}\right] \quad \text{Eq. 16}$$

$$\sigma = \begin{cases} 0.07 & k \leq k_p \\ 0.09 & k > k_p \end{cases} \quad \text{Eq. 17}$$

JONSWAP spectrum can also be used to identify the wavelength of the peak in the spectrum using the following:

$$k_p = \frac{2\pi\alpha_J}{H_s} \left[\frac{rad}{m}\right] \quad \text{Eq. 18}$$

when α_J is equal to 0.023.

To describe the wave spectra over a two-dimensional space field, we need to consider the directional spreading function. The directional spreading function is a normalization parameter for the power spectrum that is used to apply the power spectrum on two dimensions. It is a function of the frequency (or the wavenumber) and the angle that defines the direction over the two-dimensional space. The directional spreading function defined by [15] after modified into a function of the wavenumber, k, while considering the dispersion relation approximation for deep water is used. Accordingly, the directional power spectrum obtained is:

$$E(k,\theta) = S(k)G(k,\theta) \quad \text{Eq. 19}$$

where the directional spreading function is:

$$G(k,\theta) = \frac{2^{(2S-1)}\left|cos\left(\frac{\theta}{2}\right)\right|^{2s}}{\pi} \quad \text{Eq. 20}$$

the parameter s is:

$$s(k) = \begin{cases} s_{max}\left(\frac{k}{k_p}\right)^5 & k \leq k_p \\ s_{max}\left(\frac{k}{k_p}\right)^{-2.5} & k_p < k \end{cases} \quad \text{Eq. 21}$$

and s_{max} is the maximum value of s.

2.3 Data Simulation

The data used to describe the gravity waves is the simulated images of the sea surface elevation. The dimension of the sea surface images is 500 square meters with a 5-meter resolution. Accordingly, each image contains 101X101 pixels representing the sea surface's height relative to the still water line. The simulation of the gravity waves was performed by using Matlab software, based on the JONSWAP power spectrum formula as a function of the wavenumber, k, and the directional spreading function as described in Eqs. 13-18 and 19-21, respectively [4,15]. All the parameters used for the simulation are detailed in Table 1.

Table 1. The parameter used for the gravity wave simulation

Parameter	Symbol	Value
JONSWAP power spectrum parameters	β	1.25
	γ	3.3
	α_J	0.023
Distribution spreading function parameters	s_{max}	100
	θ	$(-90°) - (90°)$
Number of harmonics	N_k	500
Depth	h	$500\ m$
Wavenumber	k	$0.0001 - 0.5\ rad/m$
Spectrum peak's wavenumber	k_p	$0.02 - 0.1\ rad/m$
Waves-propagate direction relative to the horizontal line of the image	θ_0	$(-30°) - (30°)$

In this study, four sets of data that differ in the waves' angle of propagation are used. Each set of data included 10,000 simulations of the sea surface, which were realized for various spectrums, while every simulated wave spectrum was defined by the peak's wavenumber (k_p), which were randomly drawn according to a uniform distribution in the range of 0.02 - 0.1 rad/m. First, we simulated images considered waves that are propagating in parallel to the horizontal line of the image, i.e., the angle of propagation (θ_0) equals 0°. Next, another set of data, but with an angle of propagation of 30° (relative to the horizontal line of the image) is created. Figure 5 illustrates these two sets of data. After creating these datasets, to simulate a more realistic

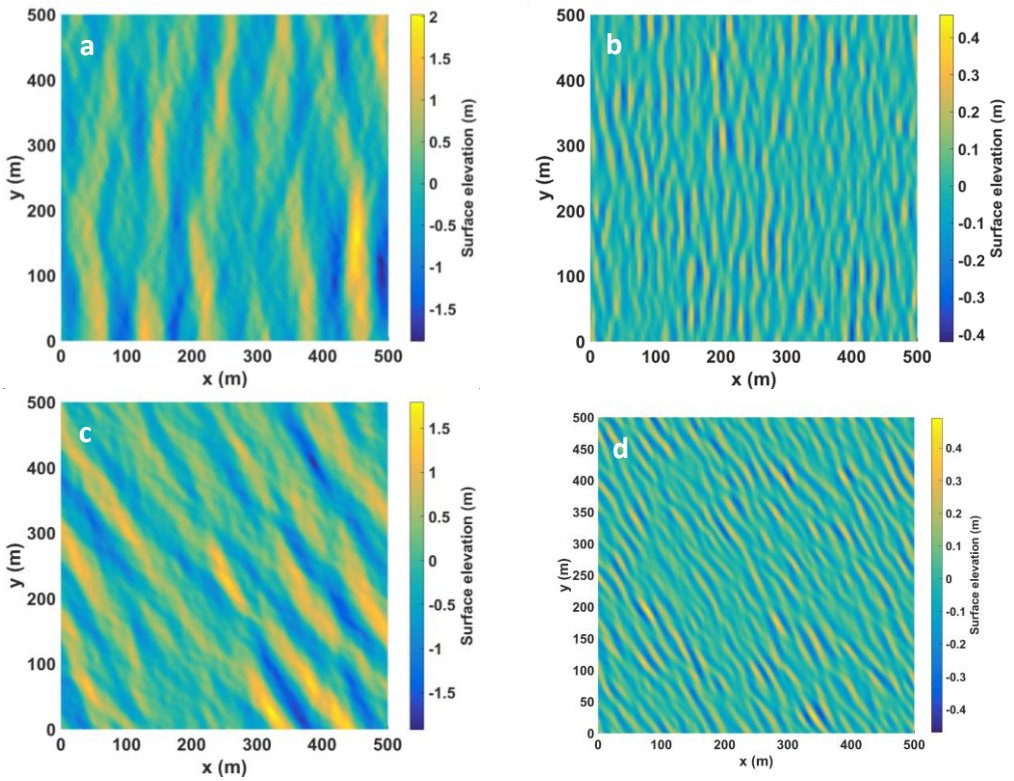

Figure 5. Examples of simulated sea surface images for different values of wavenumber and angle of propagation, Color represents the wave height. (a,c) k = 0.02 rad/m and θ_0 = 0° and 30°; (b,d) k = 0.1 rad/m and θ_0 = 0° and 30°.

input, a dataset is generated with an angle of propagation that varies around 0°, according to a normal distribution with a variance of 1.5°. Finally, the main test dataset with a random angle in the range of -30°<θ_0<30°, accordingly a uniform distribution is created. The last dataset was also used to learn the angle of propagation θ_0.

3.4 Neural Network Algorithm

As the output from the simulated sea surface images is given as a square matrix which can be interpreted as a one-channel image, the Convolutional Neural Network (CNN) architectures suit well. CNN's are being used for image processing in a variety of applications and have been improved significantly in the last few years to create pre-trained networks such as AlexNet, GoogleNet, VGGNet, etc. Due to the high computational costs of fine-tuning a pre-trained model, CNN architecture that predicts: (1) Wavenumber (2) angle of propagation of the waves from surface elevation simulation images is created from scratch. The architecture consists of a feature learning part that contains four blocks of Convolution, ReLU activation function, and max pooling. The kernels size of the convolutional layers is 9, 7, 3, 3 in the network. The Max Pooling is operated with a 2 by 2 matrix in all layers. Also, a dropout of 0.2 is added in each block to avoid over-fitting problems. Afterward, 3 fully connected layers create a prediction of wave number or angle of propagation. To learn a continuous value of spectrum peck's wavenumber (k_p) or the angle of propagation (θ_0), a cost function of the regression problem, the mean square error, is implemented, which shows good results. The optimization method is Adam optimizer.

In addition to the CNN described above, one type of transfer learning method called Domain Adaptation is also implemented (refer Figure 7). This method is essential for situations where the data does not have a ground truth to be learned on, so it uses similar data to practice on. It was first presented on digit recognition from MNIST-M (RGB) from

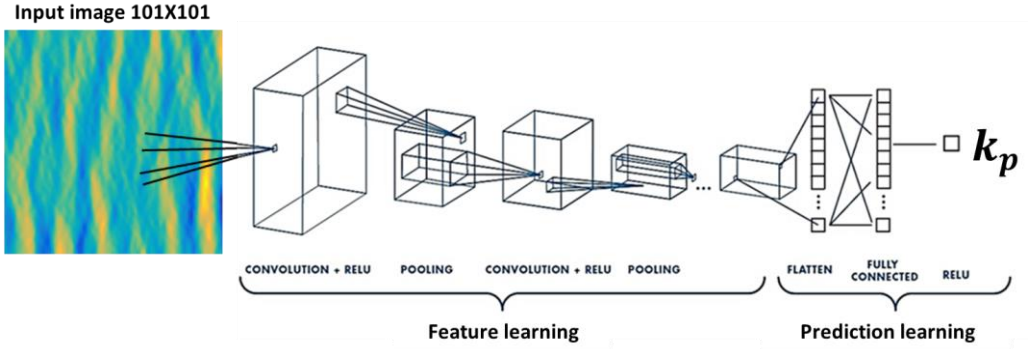

Figure 6. CNN architecture. Input image enters the feature learning parts that consist of 4 blocks of Convolution, ReLU, and max pooling. Afterward, the embedded features enter a 3 fully connected layer to generate one output neuron as the prediction. The loss function is MSE.

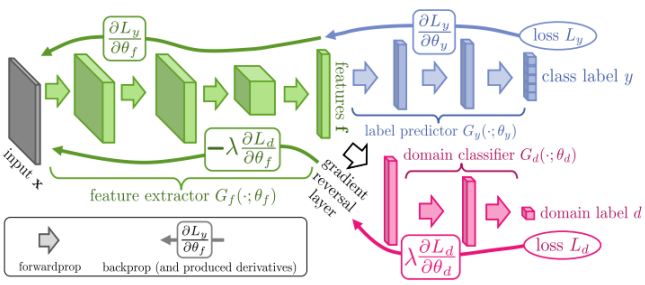

Figure 7. Visualization of domain adaptation method we used in the study [16].

learning on MNIST (grayscale) [16]. Although there is no lack of data in the network, the following method is important for future implementation on real-life predictions. Briefly, the method takes both types of images, for example, grayscale with labels and RGB without labels. Each group is given a label of type (zero and one respectively). Both groups enter the feature learning part as usual, but only the group with the labels continues to the fully connected prediction layer, as well as to another fully connected layer that classifies whether the image is RGB or grayscale. RGB images enter only the feature learning and the classification layers, as it does not have proper ground truth. As the forward propagation fails in predicting the information about RGB digit recognition, the main advantage is in the backpropagation. Using a gradient reversal layer, where a minus sign is attached to the gradients, the network can learn patterns that are not regarded to the type of the image (grayscale or RGB). The images with θ_0 = 0° angle of propagation as the grayscale images and the θ_0 = 30° angle of propagation as the RGB images are used for the training of the following network.

3. Results

The results obtained from the trained network are discussed in the following chapter. First, the network trained on the group of 0° angle of propagation, images are divided into training, validation, and test sets. As expected, the learning converges fast as only 2-5 epochs were needed for this simple prediction (Figure 8a). Next, a network with a domain adaptation section was added, and images from both 0° and 30° were used in the training stage, as explained in section 3. This method shows lower accuracy on the test set, and the convergence was slower, and about 15-20 epochs were needed (Figure 8b). Last, the model was trained on both 0° and 30°. The learning process of this stage is similar to the process observed for θ_0 = 0° images. The best weights of each learning stage were saved for testing on the main test dataset.

Figure 9 shows the predicted wavenumbers against the ground truth when using each one of the three weights described above, in other words, this verifies whether the network can generalize to predict wave number from images with an angle of propagation it has never studied on.

Figure 9 shows different correlations for each method as well as different scatter. Using weights from learning just on 0° may seem to be fine when looking at the correlation (about 83%) but observing the scatter, one can see a significant overestimation problem which degenerates the use of these weights for this purpose. In contrast, observing the predictions from weights of learning through 0° and 30° shows a very good correlation (97%), as well as a low,

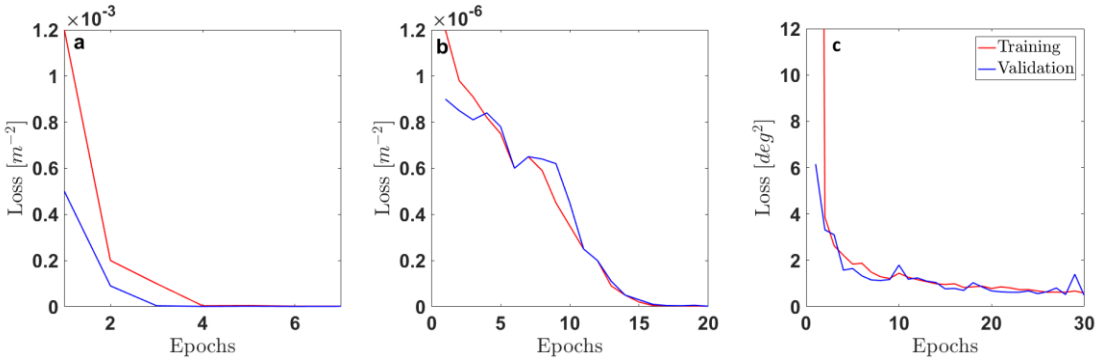

Figure 8. Learning curves - **Red** – Training. **Blue** – Validation for (a) learning on just 0°, (b) domain adaptation, and (c) angle prediction.

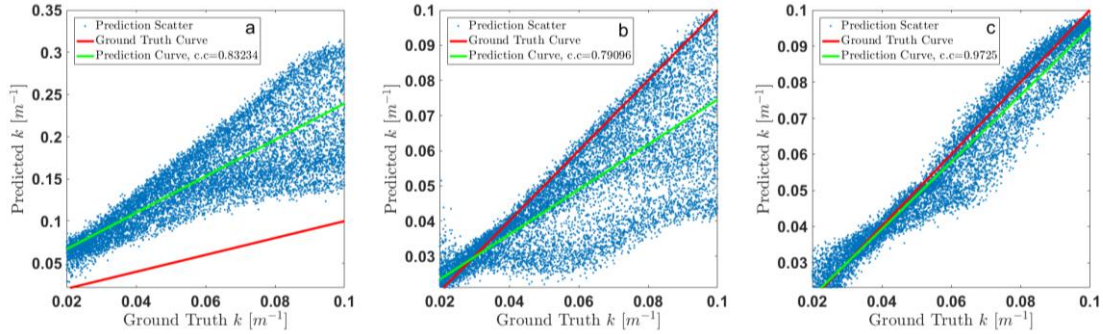

Figure 9. Predictions of wavenumber for images containing wave propagating in a random angle of propagation between 0° and 30°. **Red** curve – ground-truth value (slope 1), **Green** curve – linear regression calculated from network predictions (**Blue** dots). (a) Weights from learning just on 0°. (b) Weights from domain adaptation method. (c) Weights from learning on both 0° and 30°.

scatter of results and a good linear regression fit. Last, Figure 8b shows the domain adaptation prediction which has the lowest correlation (79%) but estimates better than the weights calculated on just one angle. The scatter of the results on both one-angle weights and domain adaption are much larger than those of the two angles weight. Besides, the error seems to arise when waves are becoming shorter (higher wavenumber) for each one of the methods. Next, a small variation in the angle of propagation in the training set is used as an input to analyze if it can improve the generalization of the network. This is done by learning on a training set that contains 0° ± 5° where the angle of propagation is Gaussian about zero with a variance of 1.5°, which mean that most images are within 0° ± 1.5°.

In Figure 10, we can see that generalization can be achieved using a small variation in the angle of propagation. Results show a similar correlation to that obtained by weights from learning both on 0° and 30°. Also, the scatter of the prediction is relatively small as the scatter when using weights from learning on 0° and 30°. This means the network can find the patterns that are not related to the angle of propagation even if the angles are close to each other but not identical. Finally, the network to predict the angle of propagation is trained. This is done solely on the main test dataset, which was divided into train, validation, and test sets, and the same network architecture is used for the angle of propagation prediction of the waves. After about 20 epochs, a very good correlation is achieved (99%) as well as a very low scatter of the predictions in comparison to wavenumber predictions is shown in Figure 10b. Here only about 65 values of angles are available within the range in comparison to 160 values in the wavenumber range, which may explain the better accuracy of this prediction.

4. Discussion and Conclusion

In the present analysis, an effort has been made to analyze different types of models for the same purpose with a different set of training data set. The input data of surface elevation is generated using a numerical model with input parameters peak wave number k and angle of propagation θ. The images generated using the simulation are used to generate a different set of training data sets for the convolutional neural network (CNN). The network is trained to predict significant wave height h_s based on peak wave number k and angle of propagation for images of surface elevations -30°< θ_0 <30°. The conclusion from the analysis is as follows:

- Learning wave numbers on more than just one angle is generalized to predict images with different angles of propagation – even outside of the learning image range.
    - Results show very good correlations about 97% when learning from more than just one angle of propagation.
    - Scatter results are small.
- In case of lack of training data using the Domain-Adaptation method can improve prediction in comparison to learning from just one angle.
- The Neural Network gives better prediction for longer waves k < 0.06.
    - This was obtained in each of the methods we checked.
- The same architecture can be used to predict the wave's angle of propagation with a 99% correlation.
    - Learning to predict angle is taking more repetitions than the wavenumber but results in a lower scatter.
    - Lower scatter can be a consequence of more district values of angles in comparison to wavenumber.

6. Limitations and Future Work

This study's conclusions could influence the design of neural networks that analyzes the sea surface elevation or related data to improve its performance (in particular, the design of convolutional neural networks). Besides, these

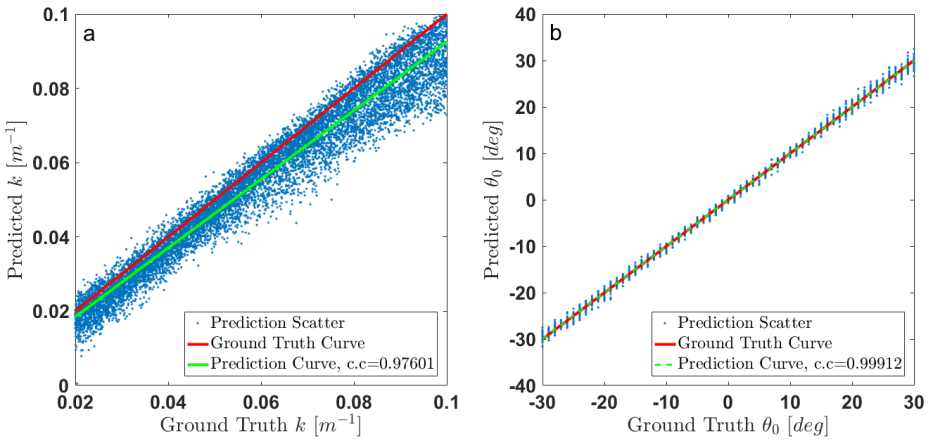

Figure 10. (a) Prediction of wavenumber for waves propagating in the range -30° to 30°, using weights calculated on an image of waves propagating in 0 ± 5°. **Red** curve – ground truth curve (slope 1), **Green** curve – a linear regression of the predictions (**Blue** dots); (b) Prediction of the angle of propagation against ground truth. **Blue** dots - predictions, **Green** curve - linear regression.

conclusions may help to understand which data is sufficient, and thus it can be collected efficiently.

After demonstrating the proposed waves inversion method with simulated data, it will be interesting to implement it with real data. Images of sea surface elevation can be reconstructed from various measurements [17-19]. Therefore, the proposed methods may be implemented with such data. However, it may be more useful to implement it with raw data of ocean 2D measurement instruments, such as radar, lidar, satellite, etc. These measurements contain information about the sea surface elevation but do not express it directly. Another complexity in these measurements arises from different biases and noises resulting from its mechanisms. Therefore, the waves inversion from these types of raw data is more challenging relative to inversion from sea surface elevation images.

The implementation of the proposed method with real data can be carried out by using it for the three stages of the deep learning process (if the properties of the waves can be measured using traditional methods), or for the testing stage only – after using simulated data for the training and the validation stages. This study took into account a constant depth only and used the approximation of deep water for the dispersion equation. The demonstration of the proposed method was performed under these limitations. Through its implementation with real data, these limitations do not remain relevant while the training and validation are also performed with the real data. However, for implementation with real data, after using simulated data for the training and the validation stages, the validity of the inversion method beyond these limitations is may be necessary.

The sea surface simulations used in this study considered a single JONSWAP power spectrum only – spectrum with a single peak representing a single group of gravity waves. However, the real sea surface may be composed of few groups of gravity waves, such as sea surface composed of different waves that propagate in different directions, sea surface characterized by wave spectra that contained few peaks corresponding to JONSWAP power spectrum function, or both. Moreover, a real sea surface may be composed of a superposition of different types of waves, such as gravity waves with capillary waves and 'infragravity waves' (shorter and longer waves). Therefore, it may be interesting to expand the suggested methods for inversion of a few groups or types of waves from each image.

There are many approaches for the design of neural networks. This study examined only a few CNN networks. It may be interesting to use a recurrent neural network (RNN) with 2D data that also includes time dimension. This approach may provide better prediction or a more effective learning process. Moreover, this approach may be the key for inversion of long waves such as 'infragravity waves', 'tide waves', and 'trans-tidal waves', which are extremely too long relative to radars and lidar working distance.

References

[1] FAO, The State of the World Fisheries and Aquaculture 2016. Contributing to the food security and nutrition for all, Technical Report, Food, and Agriculture Organization of the United Nations, 2016.

[2] Gangeskar, R., Verifying high-accuracy ocean surface current measurements by X-band radar for fixed and moving installations, IEEE Trans. Geosci. Remote Sens. 2018, 56, 4845-4855.

[3] Lighthill, J., Waves in Fluids, 2001, Cambridge Mathematical Library.

[4] Hasselmann, K., Barnett, T. P., Bouws, E., Carlson, H., Cartwright, D. E., Enke, K., Ewing J. A., Gienapp, H., Hasselmann D. E., Kruseman, P., Meerburg, A., Müller, P., Olbers, D.J., Richter, K., Sell, W., and Walden, H., Measurement of wind-wave growth and swell decay during the Joint North Sea Wave Project (JONSWAP), Hyd. Eng. Reports, 1973.

[5] Munk, W. H., and Carrier, G. F., The wind-driven circulation in Ocean Basin of Various shapes, Tellus, 1950, 2(3), 160-167.

[6] Reikard, G., Pinson, P., and Bidlot. J. R., Forecasting ocean wave energy: the ECMWF wave model and time series methods. Ocean Eng, 2011; 38:1089–99.

[7] Reikard, G., Integrating wave energy into the power grid: simulation and forecasting. Ocean Eng, 2013; 73: 168–78.

[8] Esteves, J. T., de Souza Rolim, G., and Ferraudo, A. S., Rainfall prediction methodology with binary multilayer perceptron neural networks. Climate Dynamics, 2018, 1–13.

[9] Pathak, J., Hunt, B., Girvan, M., Lu, Z., and Ott, E., Model-free prediction of large spatiotemporally chaotic systems from data: A reservoir computing approach. Physical Review Letters, 2018, 120(2), 024102.

[10] Gentine, P., Pritchard, M., Rasp, S., Reinaudi, G., and Yacalis, G., Could machine learning break the convection parameterization deadlock, Geophysical Research Letters, 2018, 45, 5742–5751.

[11] Kutz, J. N., Deep learning in fluid dynamics. Journal of Fluid Mechanics, 2017, 814, 1–4.

[12] Tracey, B. D., Duraisamy, K., and Alonso, J. J., A machine learning strategy to assist turbulence model development. In 53rd AIAA Aerospace Sciences Meeting, 2015, pp. 1287, Kissimmee, FL: Stanford University.

[13] Dean, R. G. and Dalrymple R. A., Water wave mechanics for engineers and scientists, volume 2. World Scientific Publishing Company, 1991.

[14] Pierson, W. J., and Moskowitz, L., A proposed spectral form for fully developed wind seas based on the similarity theory of sa kitaigorodskii. Journal of geophysical research, 69(24):5181-5190, 1964.

[15] Mitsuyasu, H, Tasai F, Suhara, T, Mizunom S, Ohkusu, M, Honda, T, and Rikiishi, K., Observations of the directional spectrum of ocean waves using a cloverleaf buoy. Journal of Physical Oceanography, 5(4):750-760, 1975.

[16] Ganin, Yaroslav, et al. "Domain-adversarial training of neural networks." The journal of machine learning research 17.1 (2016): 2096-2030.

[17] Cox C. and Munk W., Measurement of the Roughness of the Sea Surface from Photographs of the Sun's Glitter, Journal of the Optical Society of America, 1954, 44(11), pp. 838-850.

[18] Hessner, K. G., Nieto-Borge, J. C., and Bell, P. S., Nautical Radar Measurements in Europe: Applications of WaMoS II as a Sensor for Sea State, Current, and Bathymetry. In V. Barale, & M., 2007, Gade, Sensing of the European Seas Springer (19), pp.435-446.

[19] Schulz-Stellenfleth J. and Lehner S., Measurements of 2D surface elevation fields using complex synthetic aperture radar data, IEEE Trans. On Geos. And Remote Sens., 42(6), 2004, pp. 1149-1160.

Appendix

The codes and the data is available at the following link:

https://drive.google.com/drive/folders/1o8Jn7XU6u1Gbin8mYa84WPOtCNnc7GwS?usp=sharing